NATIONAL ADVISORY COMMITTEE FOR AERONAUTICS

TECHNICAL NOTE

No. 1638

EXPERIMENTAL INVESTIGATION OF THE JET-BOUNDARY CONSTRICTION CORRECTION FOR A MODEL SPANNING A CLOSED CIRCULAR TUNNEL

By M. Tucker and M. D. Rousso

Flight Propulsion Research Laboratory
Cleveland, Ohio

Washington
June 1948

NATIONAL ADVISORY COMMITTEE FOR AERONAUTICS

TECHNICAL NOTE NO. 1638

EXPERIMENTAL INVESTIGATION OF THE JET-BOUNDARY CONSTRICTION CORRECTION FOR A MODEL SPANNING A CLOSED CIRCULAR TUNNEL

By M. Tucker and M. D. Rousso

SUMMARY

The average low-speed jet-boundary constriction correction is presented for a large model spanning a closed circular tunnel. The experimentally determined variation of the local constriction correction with spanwise and chordwise location is also shown, A brief comparison with existing theory is given for the constriction correction and the induced-curvature correction resulting from lifting action.

INTRODUCTION

The large size of the power-plant installations investigated in the NACA Cleveland altitude wind tunnel relative to the tunnel dimensions results in large wall-interference effects. In order to determine accurately the free-stream drag and the critical speeds of such installations from tunnel measurements, the velocity increment resulting from the constriction effect of the tunnel walls must be evaluated.

The methods of references 1 and 2 may be used to obtain the average velocity increments for bodies of relatively simple shape in two- and three-dimensional flow. By use of more rigorous methods, reference 3 presents the local velocity corrections for symmetrical airfoils at zero lift in two-dimensional flow. The existing theory is inadequate, however, for the rigorous determination of the local or the average constriction corrections for bodies of arbitrary shape in three-dimensional flow. The tunnel boundary constriction was therefore experimentally investigated for a representative model spanning a closed circular tunnel.

The primary purpose of the experiments was to evaluate the low-speed jet-boundary constriction, or solid blockage, correction, that is, the velocity increment at the model due to the accelerating effect of the walls on the flow past the model at zero lift. The effect of the induced curvature of flow resulting from lifting action was obtained at the same time by testing the model at various angles of attack. The experimental results were correlated with the results obtained by existing theory.

PROCEDURE

The model investigated (figs. 1 and 2) has a wing span of 28 inches and an over-all length of 57 inches. Static-pressure taps are fitted along the model at the sections indicated in figure 3. The model surface pressures and the reference upstream dynamic pressure were obtained at speeds up to 150 feet per second for the model spanning a circular duct (fig. 4) with a diameter approximately one-eighth that of the altitude wind tunnel. The ratio of model cross-sectional area to duct cross-sectional area was 0.16, which is typical of the values encountered in investigations of full-scale installations in the altitude wind tunnel. The model was then mounted between end plates (fig. 2) to simulate an aspect ratio of 5.6 and investigated in the altitude wind tunnel to obtain the corresponding surface pressures and reference upstream dynamic pressures. The end-plate dimensions were determined using figure 11 of reference 4. The altitude wind tunnel with an area ratio of model cross section to tunnel cross section of 0.0024 was considered to simulate a free stream. Hereinafter "free stream" will refer to "altitude wind tunnel" and "tunnel" will refer to "duct."

The jet-boundary constriction correction is customarily presented for zero lift conditions as the quantity $(v_t - v_i)/V$ where

v_t velocity at surface of body in tunnel

v_i velocity at surface of body in free stream

V free-stream velocity

The velocity ratios v_t/V and v_i/V, and therefore the constriction correction, can be determined from the total and static-pressure measurements obtained from the tunnel and free-stream tests, respectively.

The effect of lift must also be considered in correcting test conditions to free-stream conditions. For the case of a model spanning the walls of a closed tunnel, the effect of lifting action is to induce a curvature of the flow about the model such as to increase the lift in the tunnel as compared with the lift in the free stream. In order to obtain data on the induced-curvature effects, the model was investigated in the tunnel and in the free stream at various angles of attack. The angle of attack was taken as the angle between the axis of the duct and the straight-line portion of the model fuselage.

A preliminary survey of the tunnel velocities with the model in place was made to determine the proper axial location (fig. 4) for measurement of the upstream velocity. Results of the survey are shown in figure 5. The dynamic pressure at station C was evidently influenced by the presence of the model. The dynamic-pressure increase from station A to station B would indicate a fairly rapid development of the boundary layer along the tunnel walls. Inasmuch as the entrance effect was probably small at station B, the velocity at this station was selected as being representative of the flow affecting the model and any further effect of velocity gradient along the tunnel was disregarded.

RESULTS AND DISCUSSION

Application of the jet-boundary constriction correction to free-stream drag and critical-pressure-coefficient determinations involves the use of the square of the constriction-correction velocity ratios. For convenience in application therefore, the constriction correction is presented as a ratio of the dynamic-pressure coefficients for the model in the free stream and in the tunnel. The dynamic-pressure coefficient is defined as q/q_o where

q model-surface dynamic pressure

q_o upstream dynamic pressure

The jet-boundary constriction factor f is expressed as the ratio

$$f \equiv \frac{(q/q_o)\ \text{free stream}}{(q/q_o)\ \text{tunnel}} \tag{1}$$

From the definition of boundary-constriction effects, this ratio is to be evaluated at zero lift. The constriction-correction

velocity ratios may be calculated from the constriction factor f by the following relation:

$$\frac{V_t - V_i}{V} = \frac{V_i}{V}\left(\sqrt{\frac{1}{f}} - 1\right) \qquad (2)$$

The jet-boundary constriction factor defined in equation (1) has been plotted in figure 6 for the various model sections at several angles of attack. Chordwise locations of the pressure taps used are indicated by the circles. Zero total lift for the model occurred at an angle of attack of approximately 0°. Data for the other angles of attack were included in these plots inasmuch as such data are not generally available in the literature and may be of interest. As shown in figure 6, the constriction factor varies appreciably with chordwise and spanwise location. The chordwise variation of the constriction factor over the wing surface for the most part appears consistent with the variation of wing thickness along the chord. Similar conclusions might be drawn for the variation of the constriction factor over the nacelle surfaces. The constriction factors obtained for the fuselage lower surface at section 5 (fig. 6(l)) seem extremely high when compared with values obtained at nacelle section 4 (fig. 6(j)). The fuselage lower-surface velocity distributions obtained from the tunnel tests were irregular but consistent. The data for the faired curves of figure 6 were averaged from tests at several airspeeds.

A summary of the average constriction-factor values of the curves at an angle of attack of 0° is given in the following table:

Wing:	
Upper surface	0.77
Lower surface	.79
Average	.78
Nacelles:	
Station 1	.84
Station 2	.81
Station 3	.81
Station 4	.81
Average	.82
Fuselage:	
Upper surface	.84
Lower surface	.97
Average	.91

The jet-boundary constriction factor representative of the model taken as the average of the values for the wing, the nacelles, and the fuselage is 0.84.

From data obtained at various angles of attack, the effects of the constriction and induced curvature of flow on the lift-curve slope can be isolated. From integration of the dynamic-pressure coefficients, the ratio of the lift-curve slope for the model in the tunnel to the lift-curve slope of the model in the free stream was found to be 1.76. The lift curves for these two conditions are shown in figure 7.

COMPARISON WITH EXISTING THEORY

Constriction

A comparison of the experimental values with the results of the existing theory may be of interest. In figure 7(a) of reference 3, the velocity ratio $(v_t - v_i)/V$ is given as a function of tc/h^2 for symmetrical airfoils of 12- and 24-percent thickness where

t maximum airfoil thickness

c airfoil chord

h tunnel height

When the applicable value of tc/h^2 is 0.066, the ratio $(v_t - v_i)/V$ is approximately 0.028. The average constriction factor f obtained for the wing sections, which have an average thickness of approximately 15 percent, was 0.78. By use of equation (2) and an experimentally obtained value for the wing of $v_i/V = 1.12$, the corresponding value of the ratio $(v_t - v_i)/V$ becomes 0.148, which is about five times greater than the theoretical value obtained for a wing in two-dimensional flow. The fuselage and nacelles apparently have a large effect on the constriction velocity about the wings.

The question thus arises as to the possibility of computing the incremental velocities (that is, increment due to the tunnel) for the component parts of the model and combining these by superposition to obtain the over-all velocity increment. The component velocity-increment ratios for incompressible flow were obtained from equation (22) of reference 2, which is given in the notation of this paper for a tunnel having a height-to-breadth ratio of 0.7 as follows:

$$\frac{v_t - v_i}{V} = \frac{km}{(bh)^{3/2}} \tag{3}$$

where

K 0.74 for two-dimensional wing spanning tunnel breadth
0.52 for two-dimensional wing spanning tunnel height
0.96 for streamlined body of revolution

m volume of model or component part

b breadth of tunnel test section

h height of tunnel test section

The assumption was made that equation (3) is applicable to a closed circular tunnel, the area bh being the cross-sectional area. The value of K for a wing spanning a circular tunnel was taken as 0.63, the average of the values listed for a two-dimensional wing.

For the purpose of calculation, the model (figs. 1 and 2) is regarded as consisting of two parts: (1) the wing and (2) the fuselage and the nacelles. The volumes of the wing, the fuselage, and the nacelles were 0.225, 0.698, and 0.250 cubic foot, respectively. The cross-sectional area of the circular duct was 4.79 square feet. From equation (3) the ratio $(v_t - v_i)/V$ for the wing is 0.0135 when K is 0.63; similarly, the ratio $(v_t - v_i)/V$ for the fuselage plus the nacelles is 0.0868 when K is 0.96. The assumption is now made that the effective velocity-increment ratio is the sum of these ratios or 0.100. The ratio v_i/V for the model was 1.06. When the wake constriction is assumed to be negligible, the corresponding constriction factor f from equation (2) is 0.835, which is in agreement with the experimental value of 0.84.

In view of the assumptions entailed in the calculation, the supposition that such agreement between calculated and experimental values will be obtained for other models cannot be made. The unreliability of the various theories when applied to the component parts of large models is shown by a comparison of the values 0.0135 and 0.028, obtained from references 2 and 3, respectively, for the wing velocity ratio $(v_t - v_i)/V$.

Induced Curvature

For a model spanning a closed tunnel, lifting action induces a curvature of flow about the model. The induced-curvature correction is defined as the ratio of lift of a model in a tunnel to its

free-stream lift at the same geometric angle of attack. The theoretical induced-curvature corrections obtained by Rosenhead for a flat plate in a two-dimensional tunnel are given in figure 22 of reference 1 as a function of lift coefficient and chord to tunnel-height ratio. The analysis given in reference 5 indicates that, as far as induced curvature effects are concerned, the equivalent two-dimesnional height for a wing spanning a closed circular tunnel is 0.843 times tunnel diameter. For the model investigated, the applicable chord-height ratio is 0.61; for small lift coefficients, the theoretical induced-curvature correction for a flat plate in two-dimensional flow is therefore 1.13.

A wing spanning a closed circular tunnel is shown in reference 5 to approximate a wing of infinite aspect ratio. If the lift-curve slope for the model in the free stream is corrected to infinite aspect ratio using the E factor $\left(\frac{\text{wing semiperimeter}}{\text{wing span}}\right)$ of reference 6, the ratio of lift-curve slope for the model in the tunnel at infinite aspect ratio to lift-curve slope for the model in the free stream at infinite aspect ratio becomes 1.30. Part of this increase of lift in the tunnel as compared with the lift in the free stream results from the increased dynamic pressure acting on the model in the tunnel because of the tunnel-wall constriction. From the definition of constriction factor f, it is seen that this increased dynamic pressure is $1/f$ times the dynamic pressure acting on the model in the free stream. The rest of the increase of lift in the tunnel is then attributable to the induced curvature of flow. The induced-curvature correction is therefore obtained by multiplying the constriction factor f by the ratio of lift-curve slopes.

A question arises as to the proper value of constriction factor to be used in obtaining the induced-curvature correction. Inasmuch as the nacelles and fuselage contribute to the lift, it appeared reasonable to use a weighted average of the constriction factors of the wing, the nacelle, and the fuselage based on the percentage of lift contributed by each. For the model investigated, the wing contributed approximately 76 percent of the total lift. When a weighted average constriction factor of 0.80 was used, the induced-curvature correction for the model was $1.30 \times 0.80 = 1.04$ as compared with the theoretical correction of 1.13. The effect of the tunnel-wall boundary layer, which tends to cause a loss of lift at the wing-tip sections, may partly account for the discrepancy in the theoretical and experimental values. Quantitative agreement between the corrections for a flat plate and a model of the type investigated could not be expected.

SUMMARY OF RESULTS

The results of this experimental investigation on jet-boundary constriction corrections may be summarized as follows:

1. The average low-speed jet-boundary constriction factor f defined as $\frac{(q/q_o)\text{ free stream}}{(q/q_o)\text{ tunnel}}$ was 0.84 for the configuration tested, in which the model spanned a circular tunnel and the ratio of model cross-sectional area to tunnel cross-sectional area was 0.16. Deviations of the local constriction factor from the average were appreciable.

2. Theoretical constriction corrections for the component parts of the model did not check the experimental values, which indicates that the mutual interference of these parts was apparently large. The over-all constriction correction obtained from existing theory could be brought into agreement with the experimental value, however, by use of the principle of superposition.

3. The effect of the induced curvature of flow on the lift obtained from existing theory for a flat plate in a two-dimensional tunnel was in qualitative agreement with the experimental results obtained for the model spanning a closed circular tunnel.

Flight Propulsion Research Laboratory,
National Advisory Committee for Aeronautics,
Cleveland, Ohio, March 16, 1948.

REFERENCES

1. Glauert, H.: Wind Tunnel Interference on Wings, Bodies, and Airscrews. R. & M. No. 1566, British A.R.C., 1933.

2. Thom, A.: Blockage Corrections in a Closed High-Speed Tunnel. R. & M. No. 2033, British A.R.C., 1943.

3. Perl, W., and Moses, H. E.: Velocity Distributions on Symmetrical Airfoils in Closed Tunnels by Conformal Mapping. NACA TN No. 1642, 1948.

4. Mangler, W.: The Lift Distribution of Wings with End Plates. NACA TM No. 856, 1938.

5. Vincenti, Walter G., and Graham, Donald J.: The Effect of Wall Interference upon the Aerodynamic Characteristics of an Airfoil Spanning a Closed-Throat Circular Wind Tunnel. NACA ACR No. 5D21, 1945.

6. Jones, Robert T.: Correction of the Lifting-Line Theory for the Effect of the Chord. NACA TN No. 817, 1941.

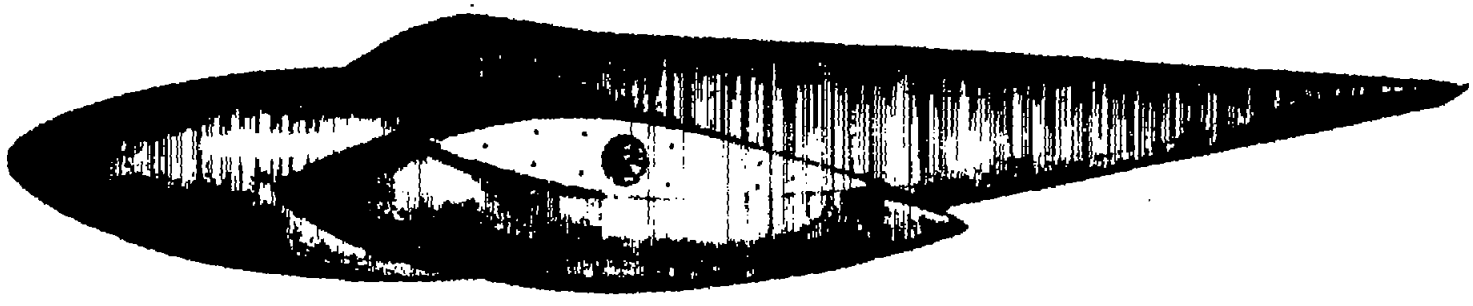

Figure 1. - Side view of model tested.

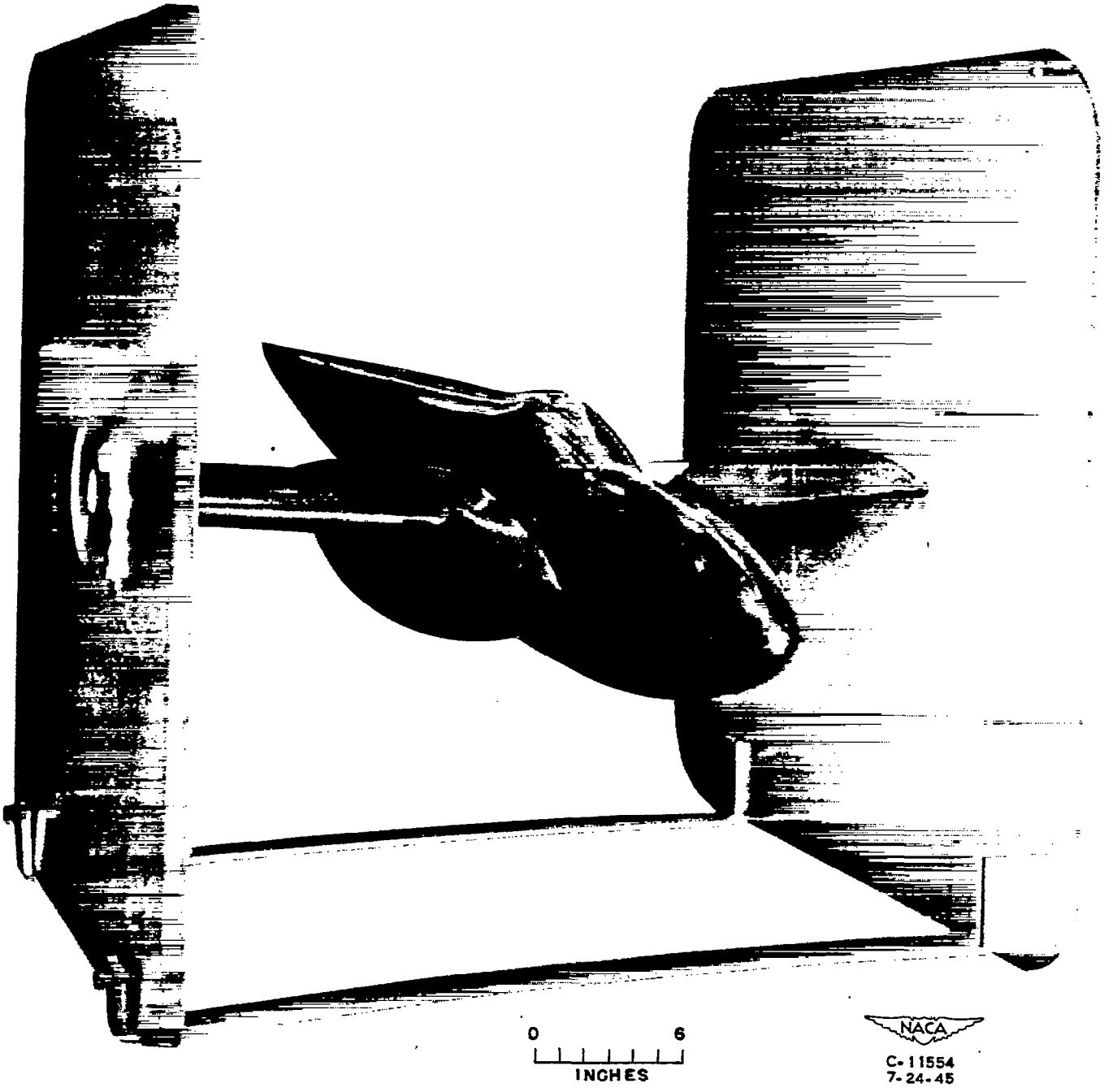

Figure 2. - Model mounted between end plates for investigation in altitude wind tunnel.

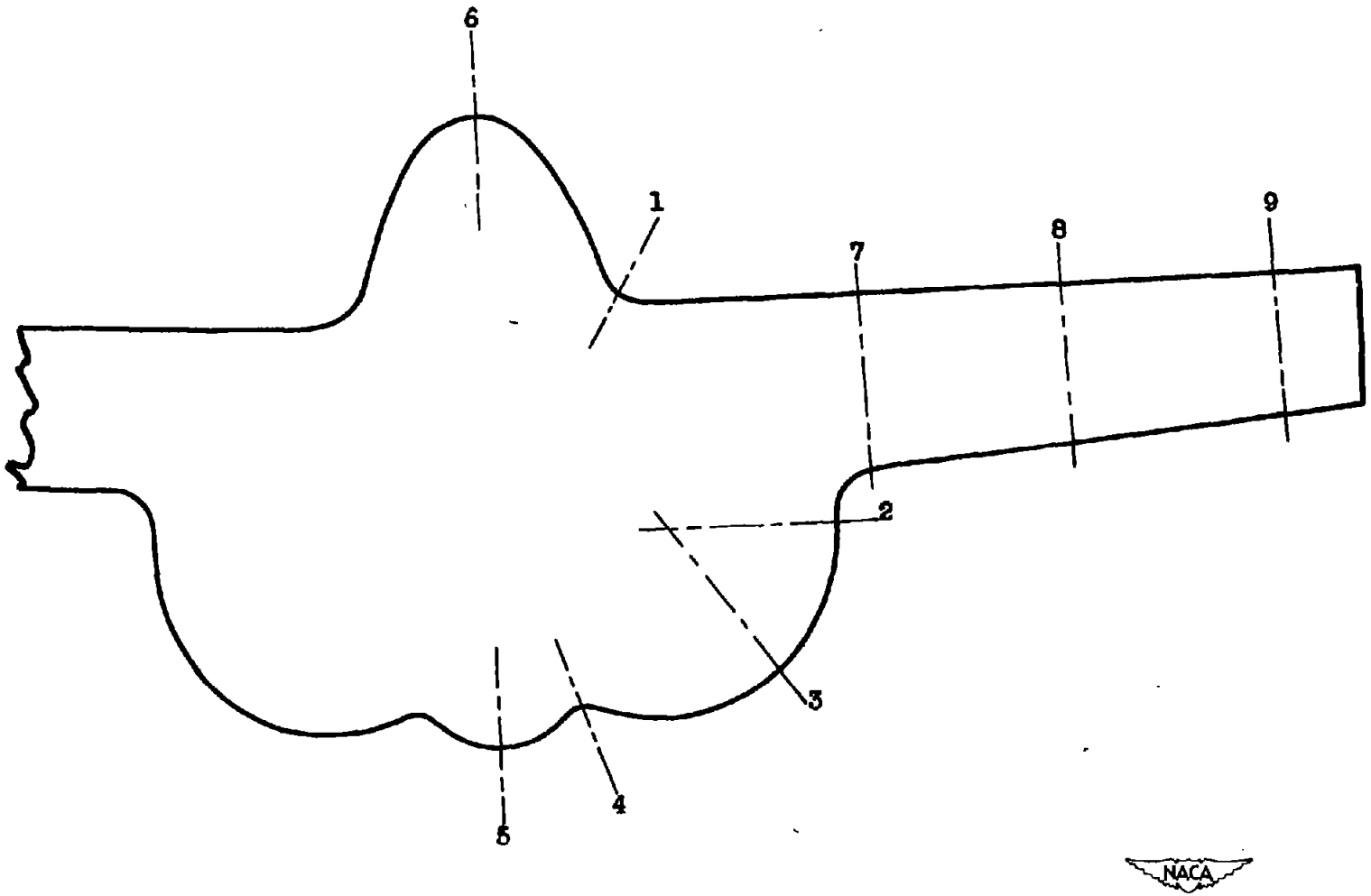

Figure 3. - Designation of sections at which pressure taps were located on surface of model.

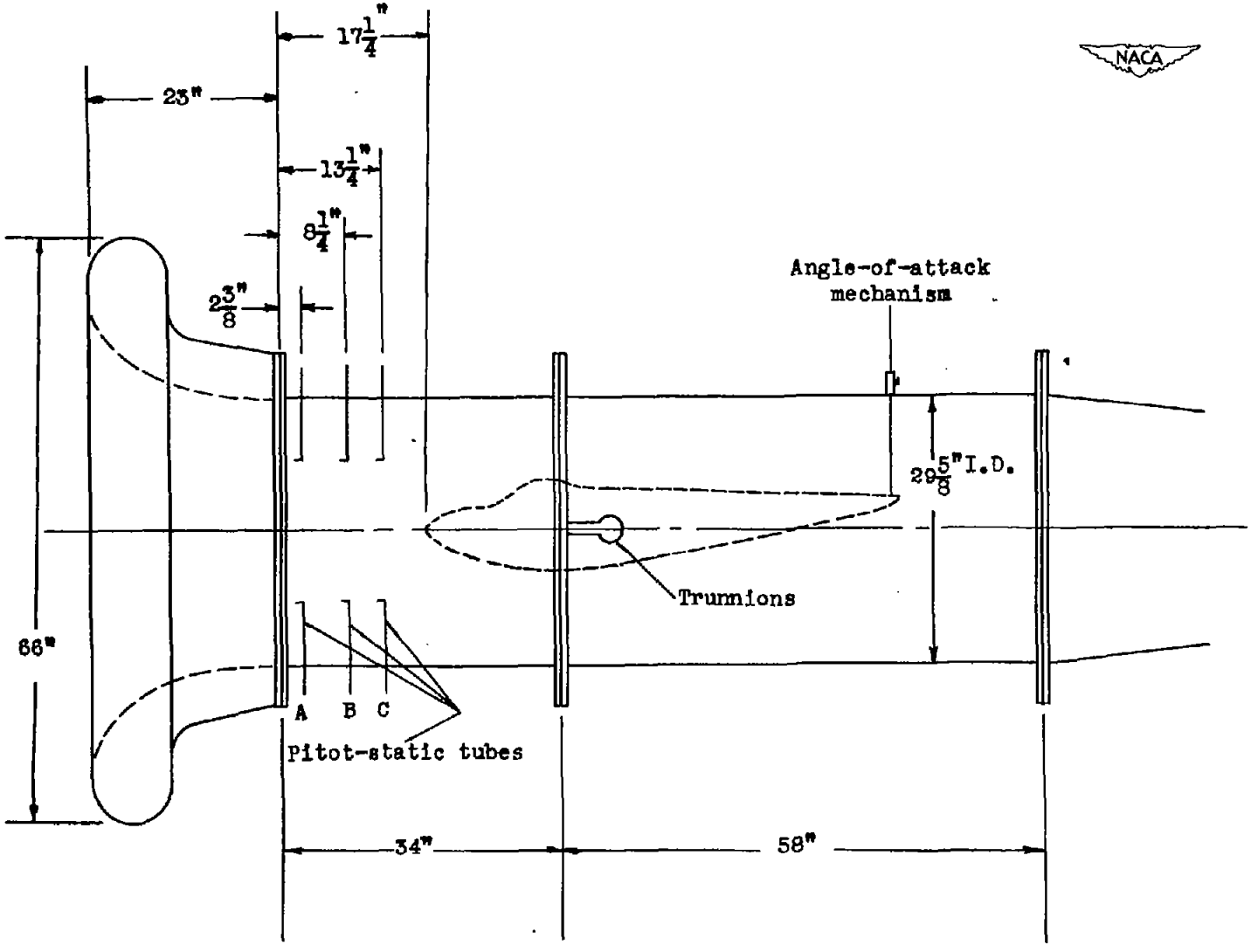

Figure 4. - Schematic diagram of circular duct used for jet-boundary constriction investigation.

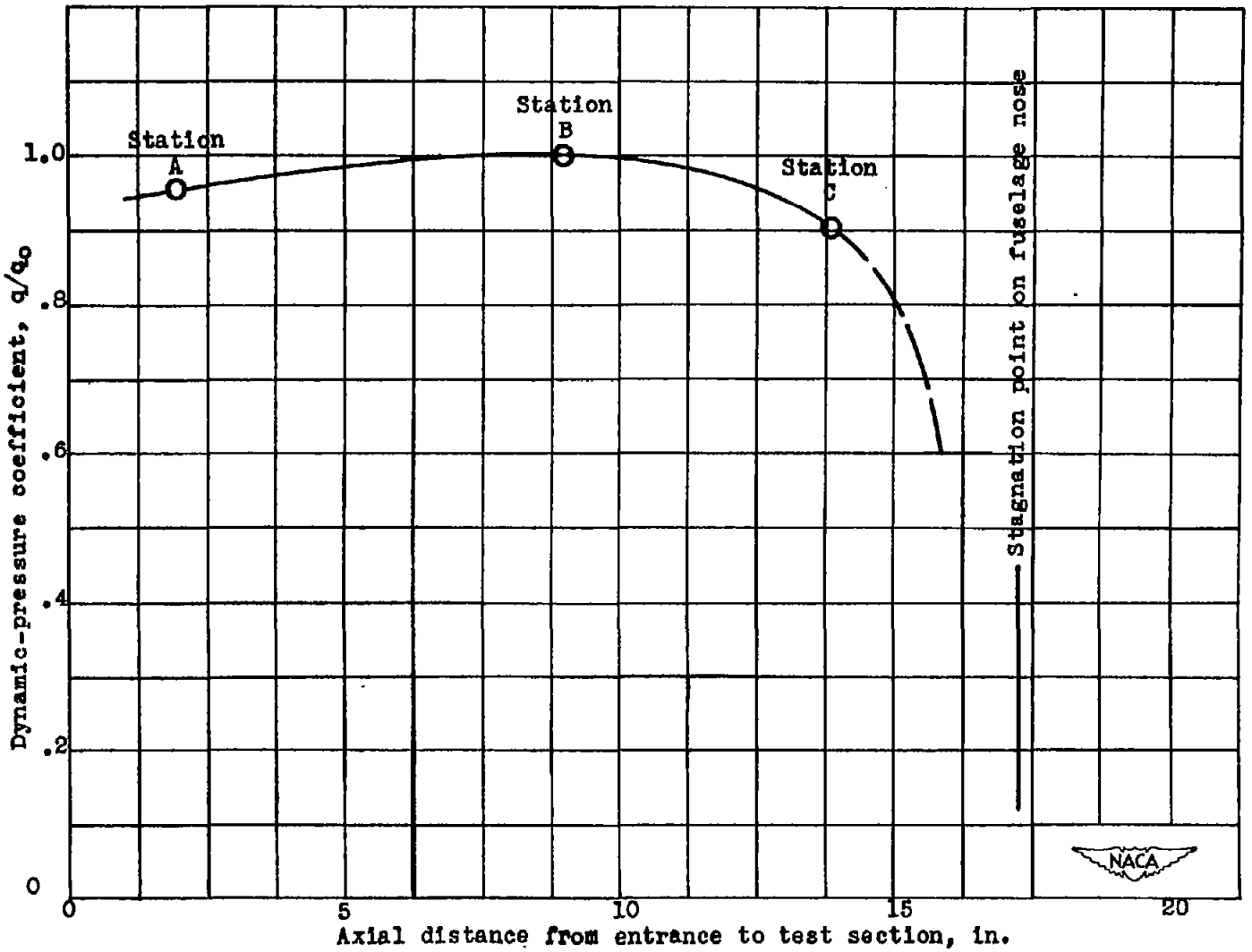

Figure 5. - Variation of dynamic pressure along axis of circular duct with model at an angle of attack of 0°.

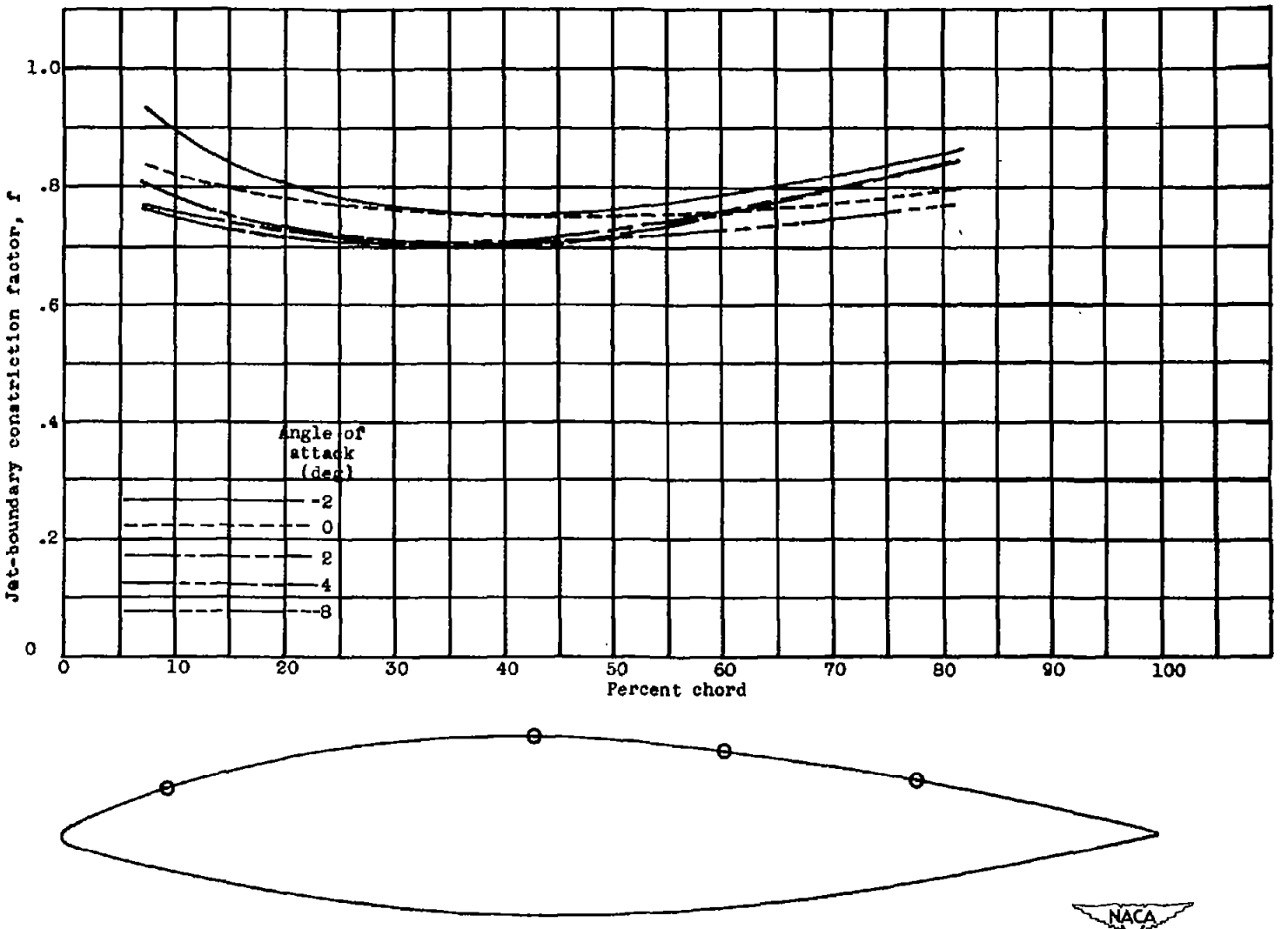

(a) Wing upper surface at section 7.

Figure 6. - Variation of jet-boundary constriction factor with angle of attack and chordwise location. (Orifice locations indicated on sketch.)

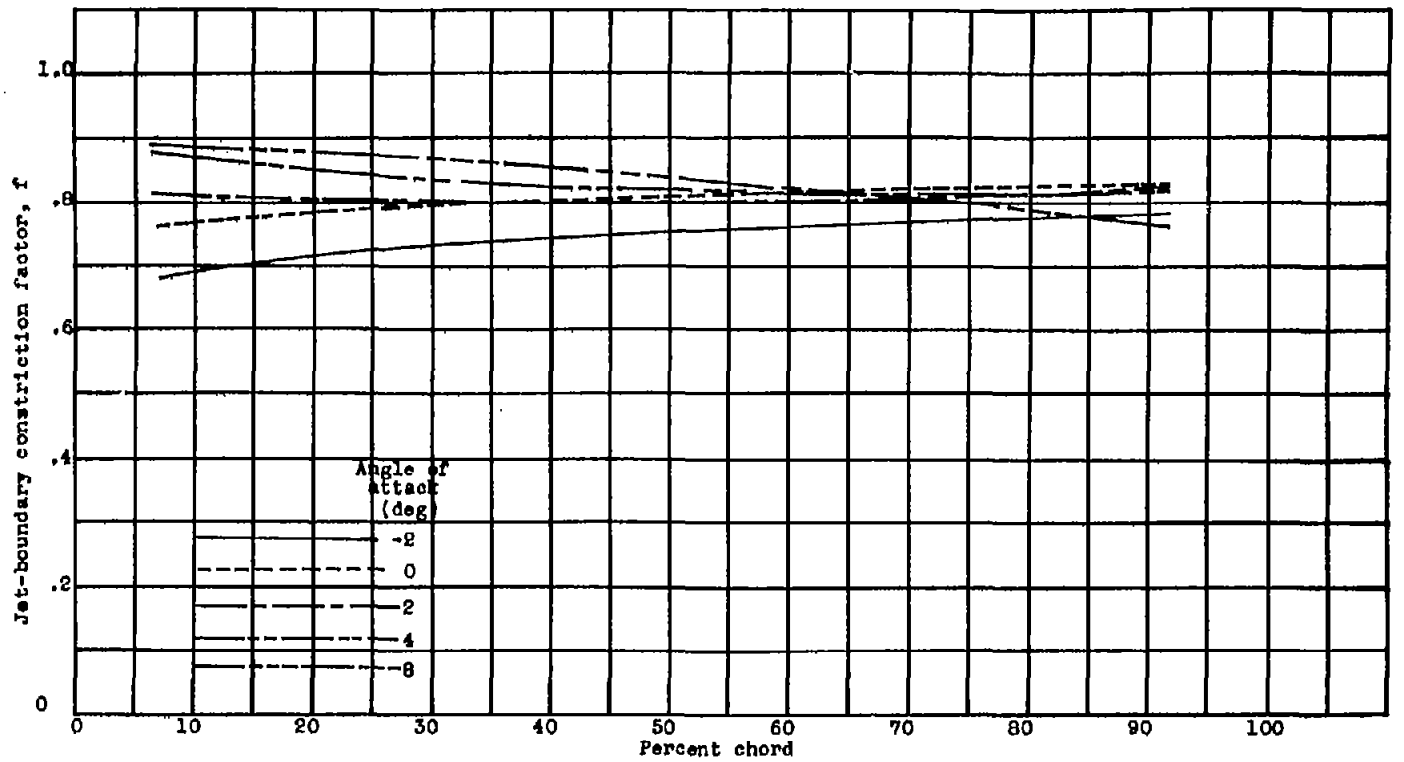

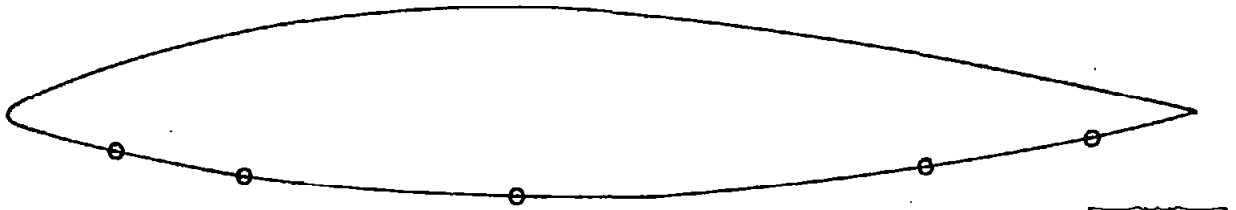

(b) Wing lower surface at section 7.

Figure 6. - Continued. Variation of jet-boundary constriction factor with angle of attack and chordwise location. (Orifice locations indicated on sketch.)

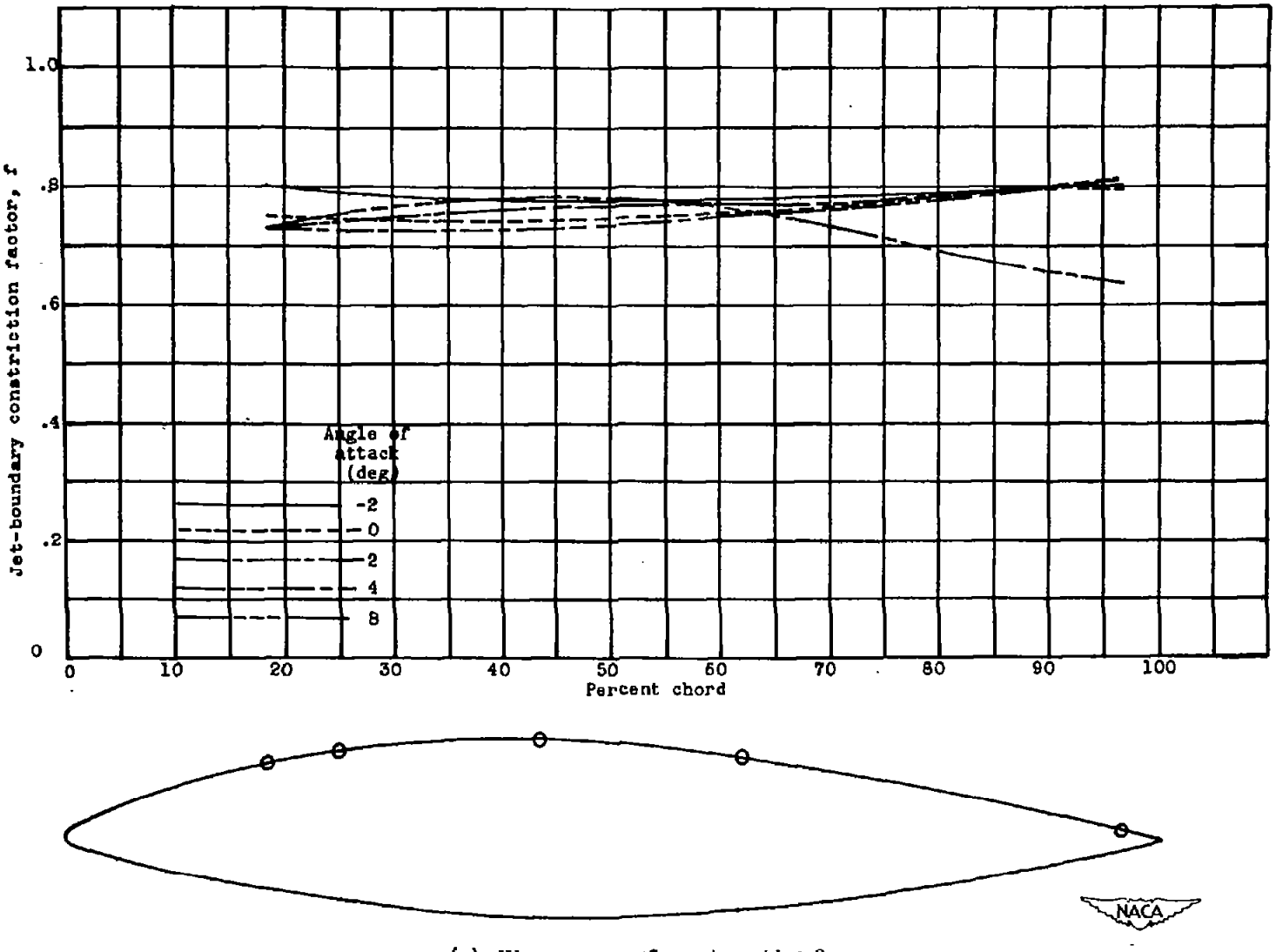

(c) Wing upper surface at section 8.

Figure 6. - Continued. Variation of jet-boundary constriction factor with angle of attack and chordwise location. (Orifice locations indicated on sketch.)

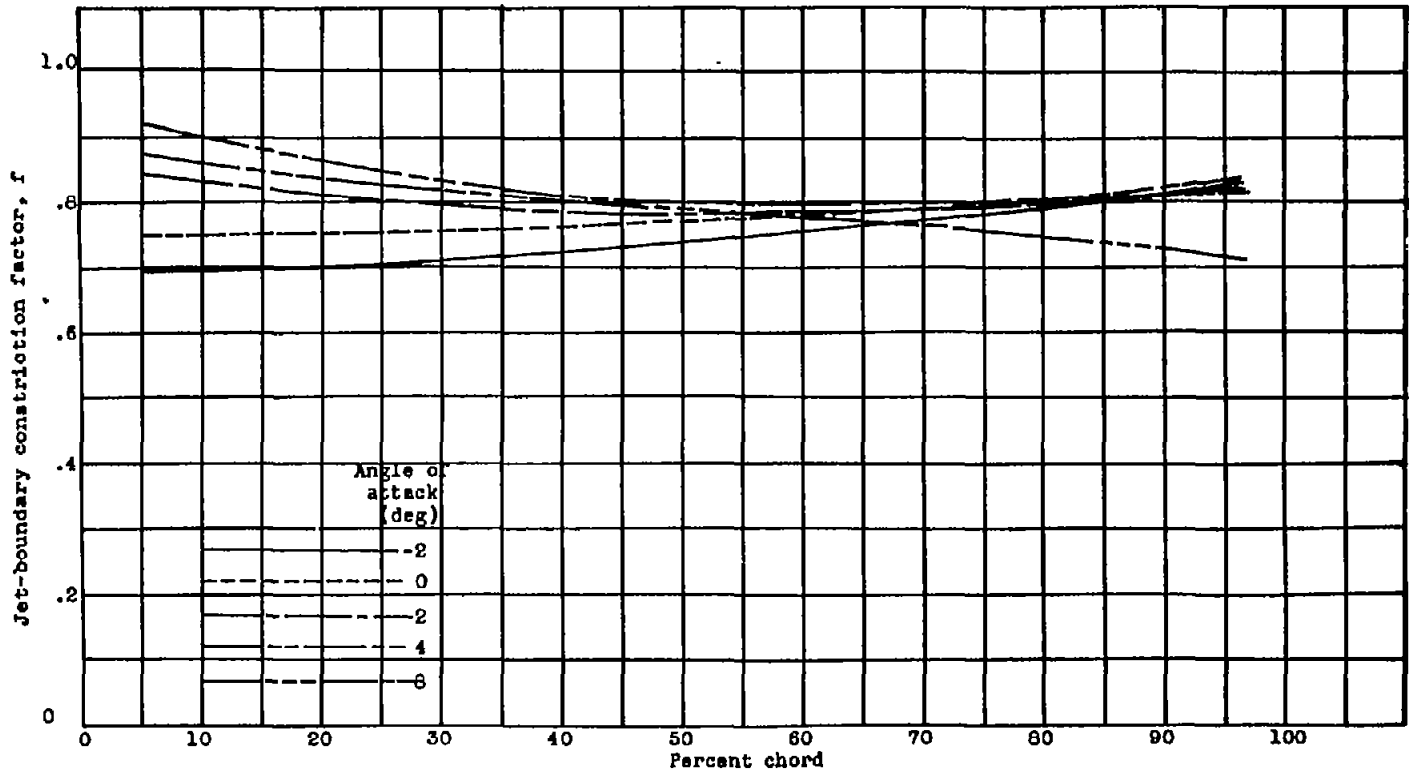

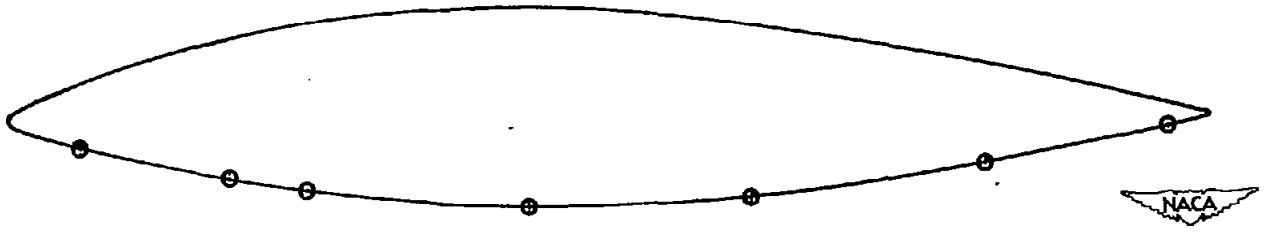

(d) Wing lower surface at section 8.

Figure 6. - Continued. Variation of jet-boundary constriction factor with angle of attack and chordwise location. (Orifice locations indicated on sketch.)

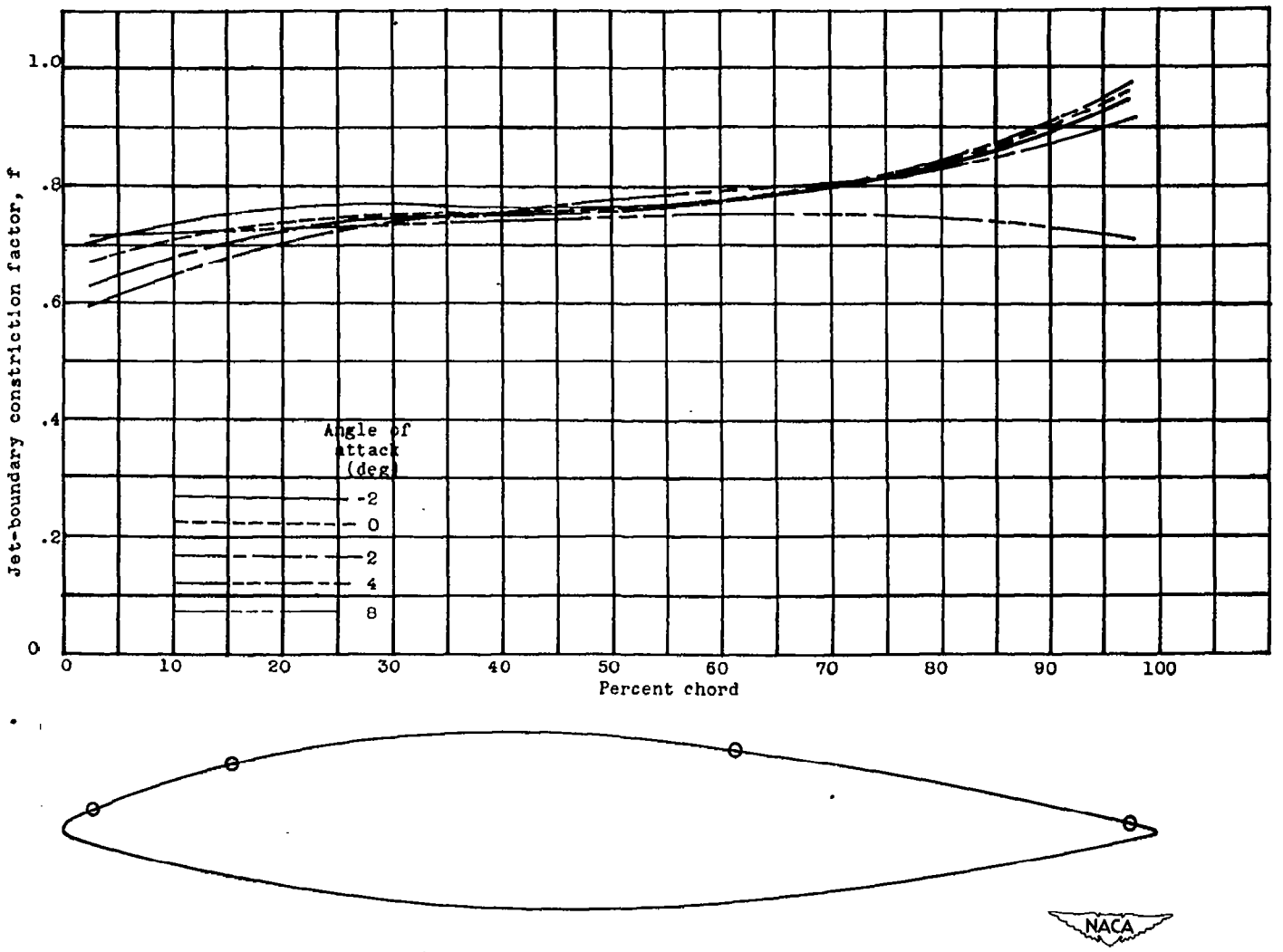

(e) Wing upper surface at section 9.

Figure 6. - Continued. Variation of jet-boundary constriction factor with angle of attack and chordwise location. (Orifice locations indicated on sketch.)

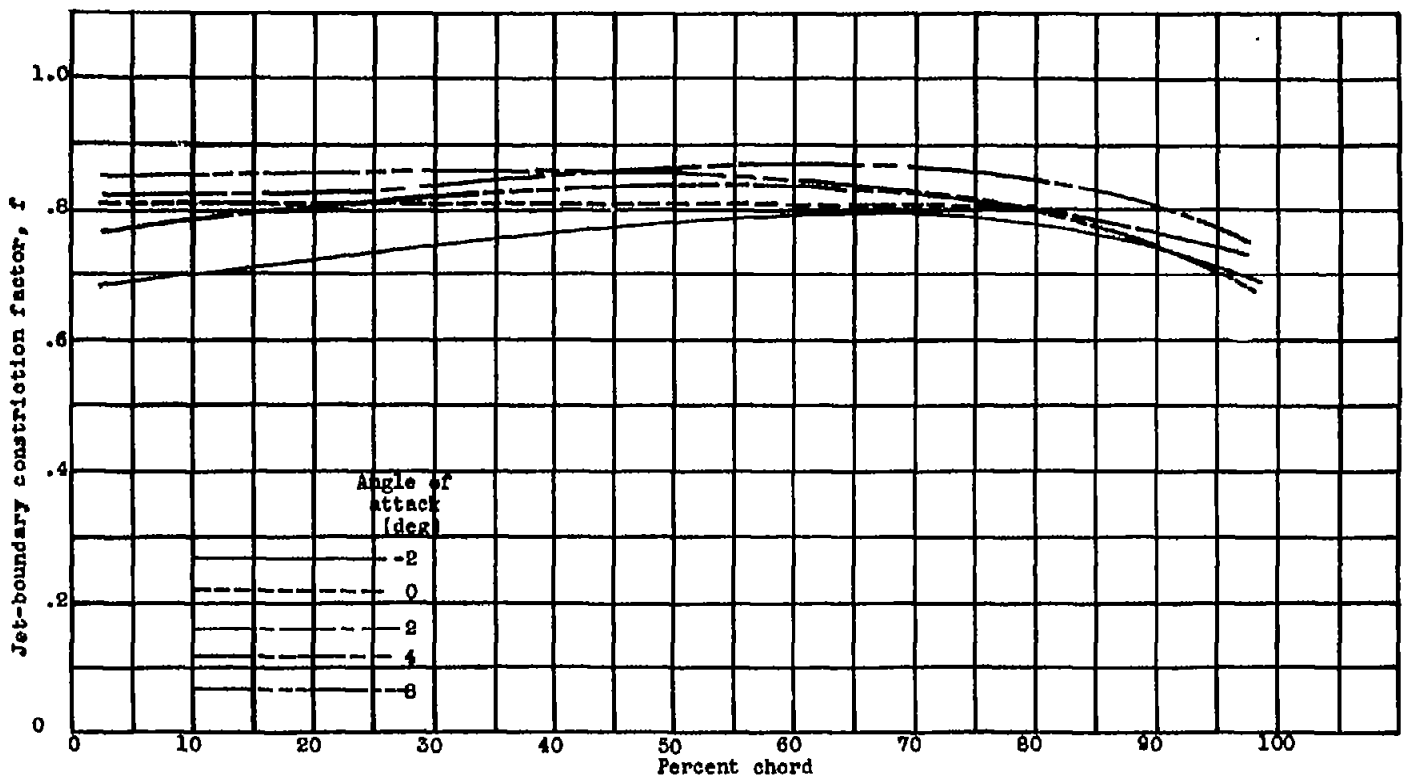

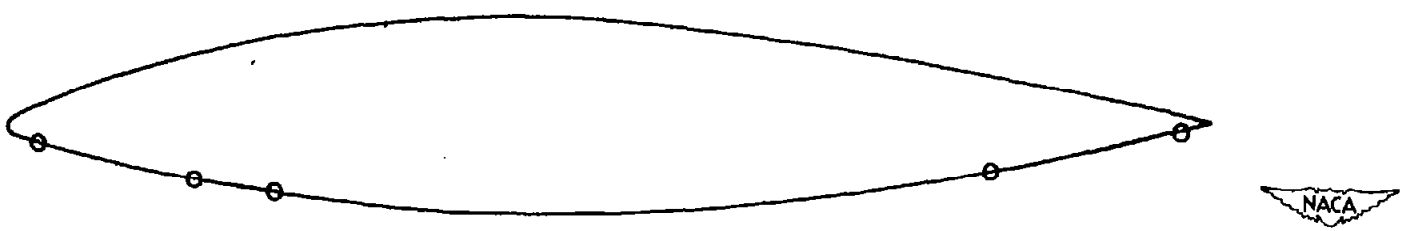

(f) Wing lower surface at section 9.

Figure 6. - Continued. Variation of jet-boundary constriction factor with angle of attack and chordwise location. (Orifice locations indicated on sketch.)

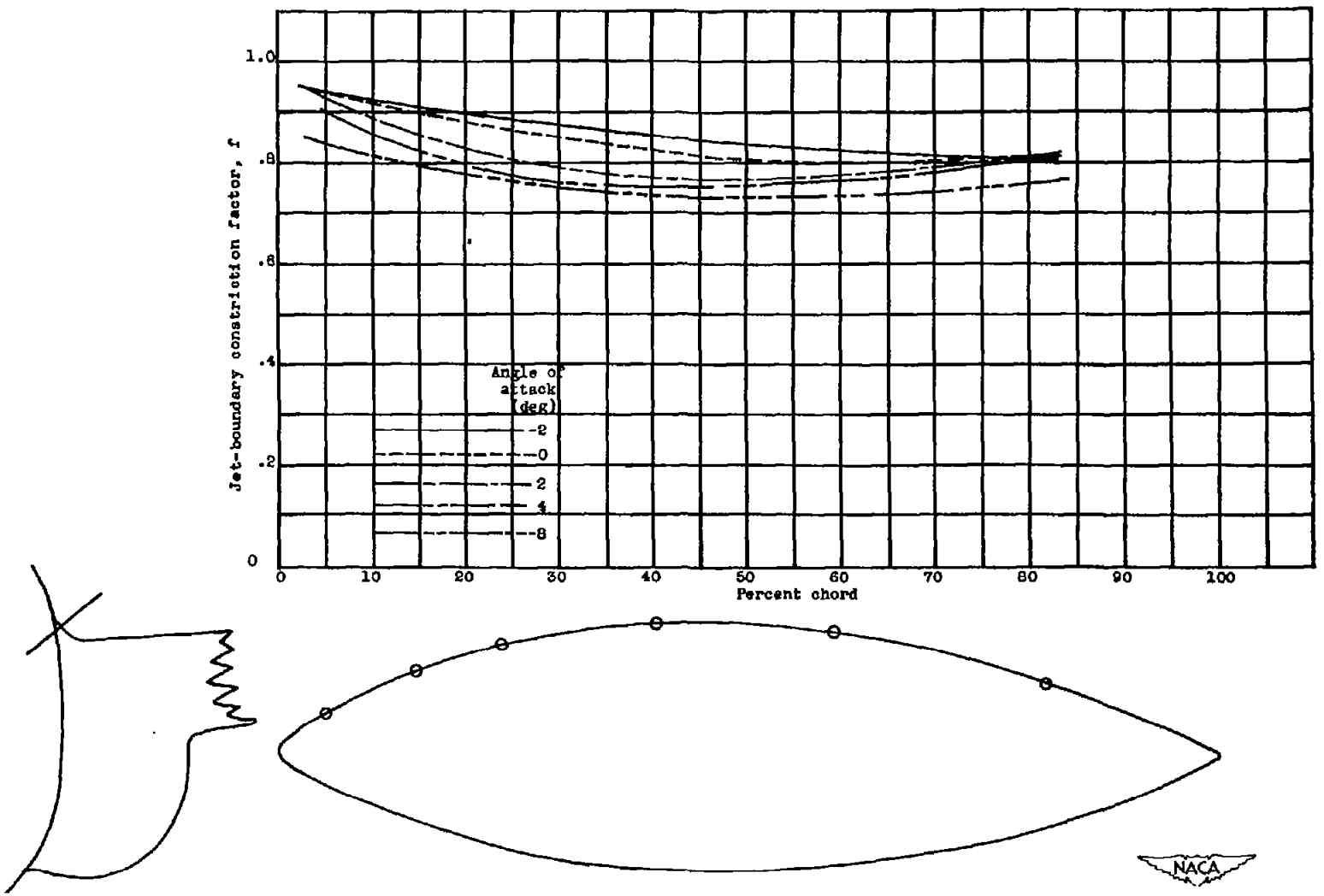

(g) Nacelles at section 1.

Figure 6. - Continued. Variation of jet-boundary constriction factor with angle of attack and chordwise location. (Orifice locations indicated on sketch.)

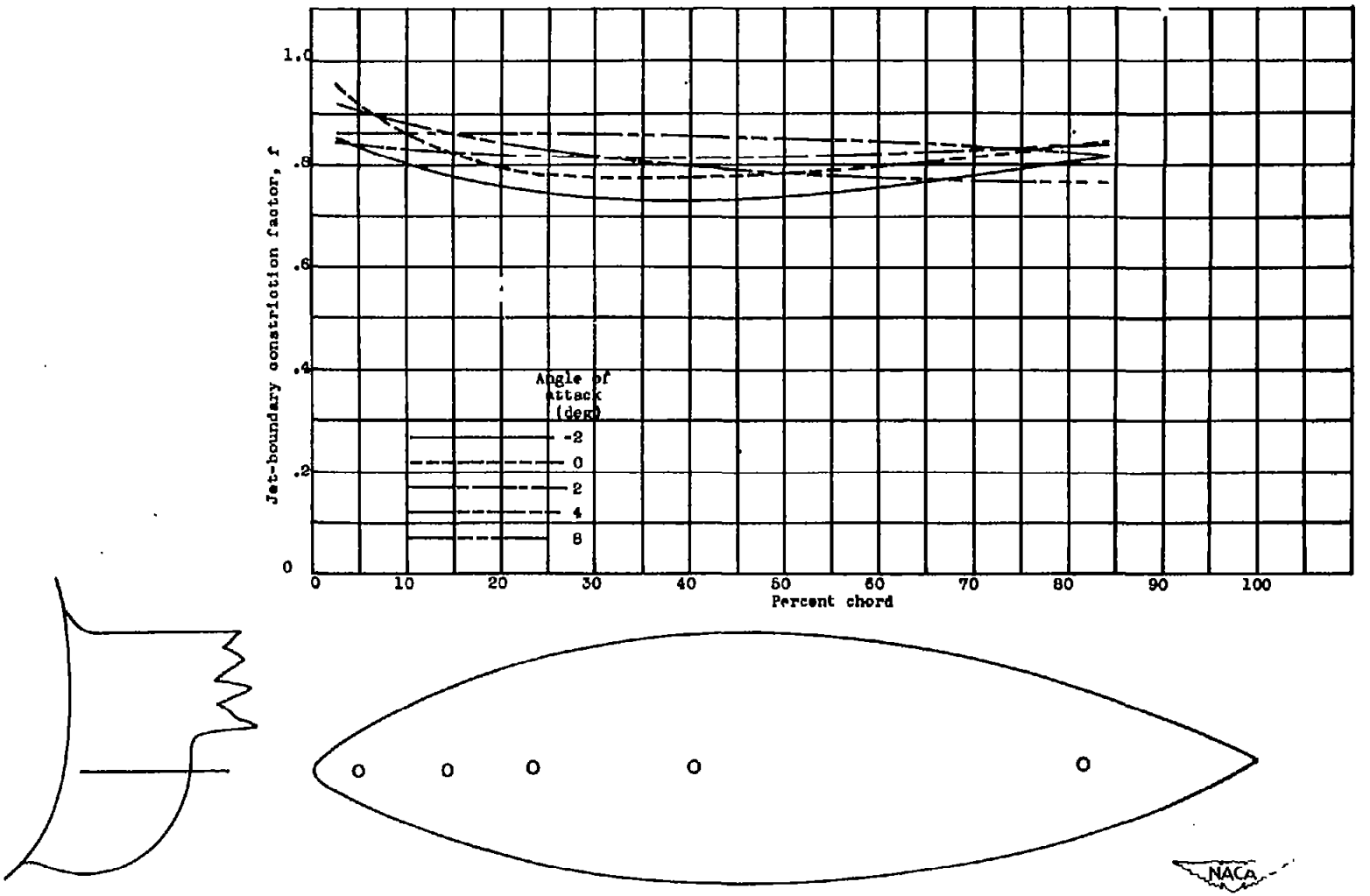

(h) Nacelles at section 2.

Figure 6. - Continued. Variation of jet-boundary constriction factor with angle of attack and chordwise location. (Orifice locations indicated on sketch.)

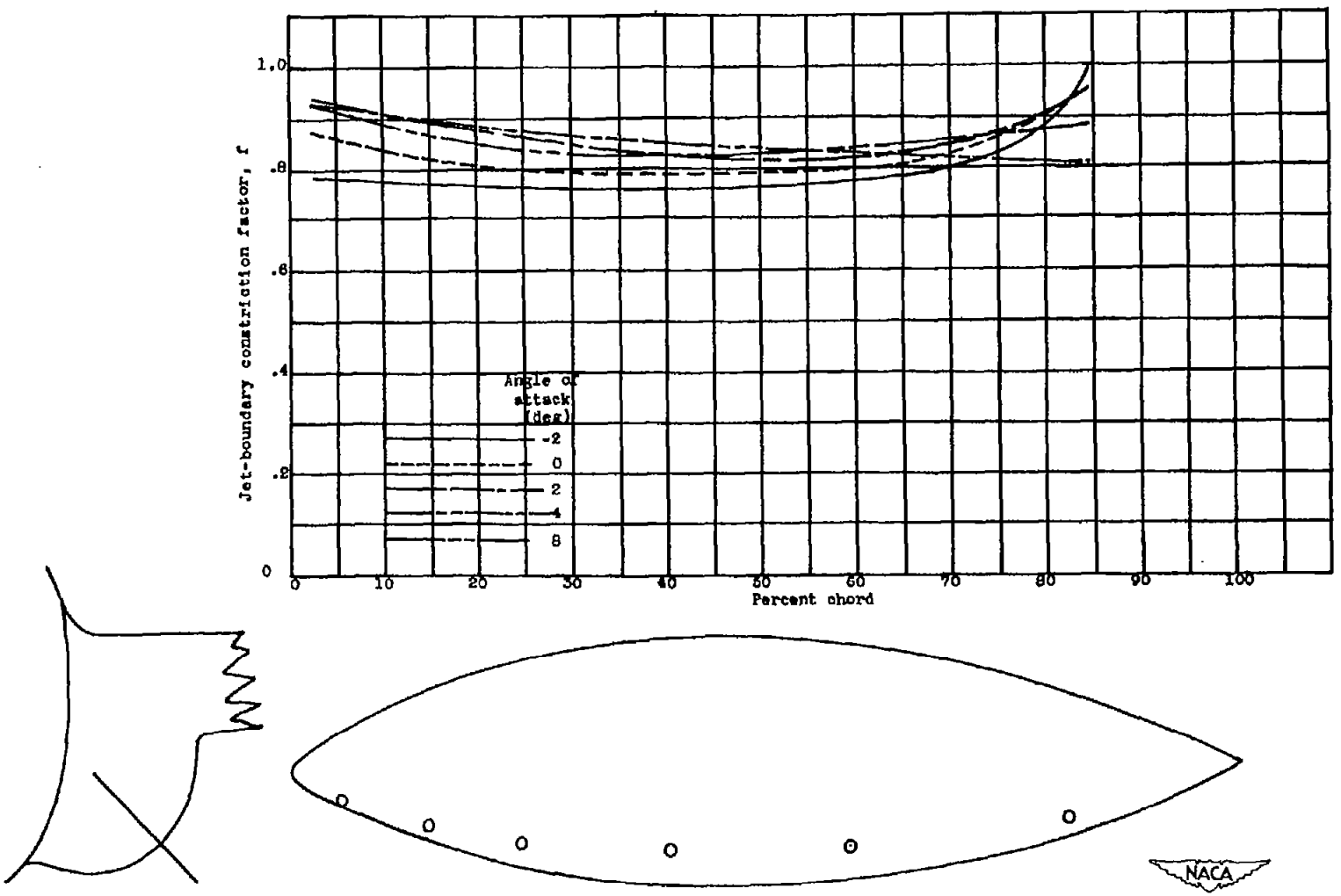

(i) Nacelles at section 3.

Figure 6. - Continued. Variation of jet-boundary constriction factor with angle of attack and chordwise location. (Orifice locations indicated on sketch.)

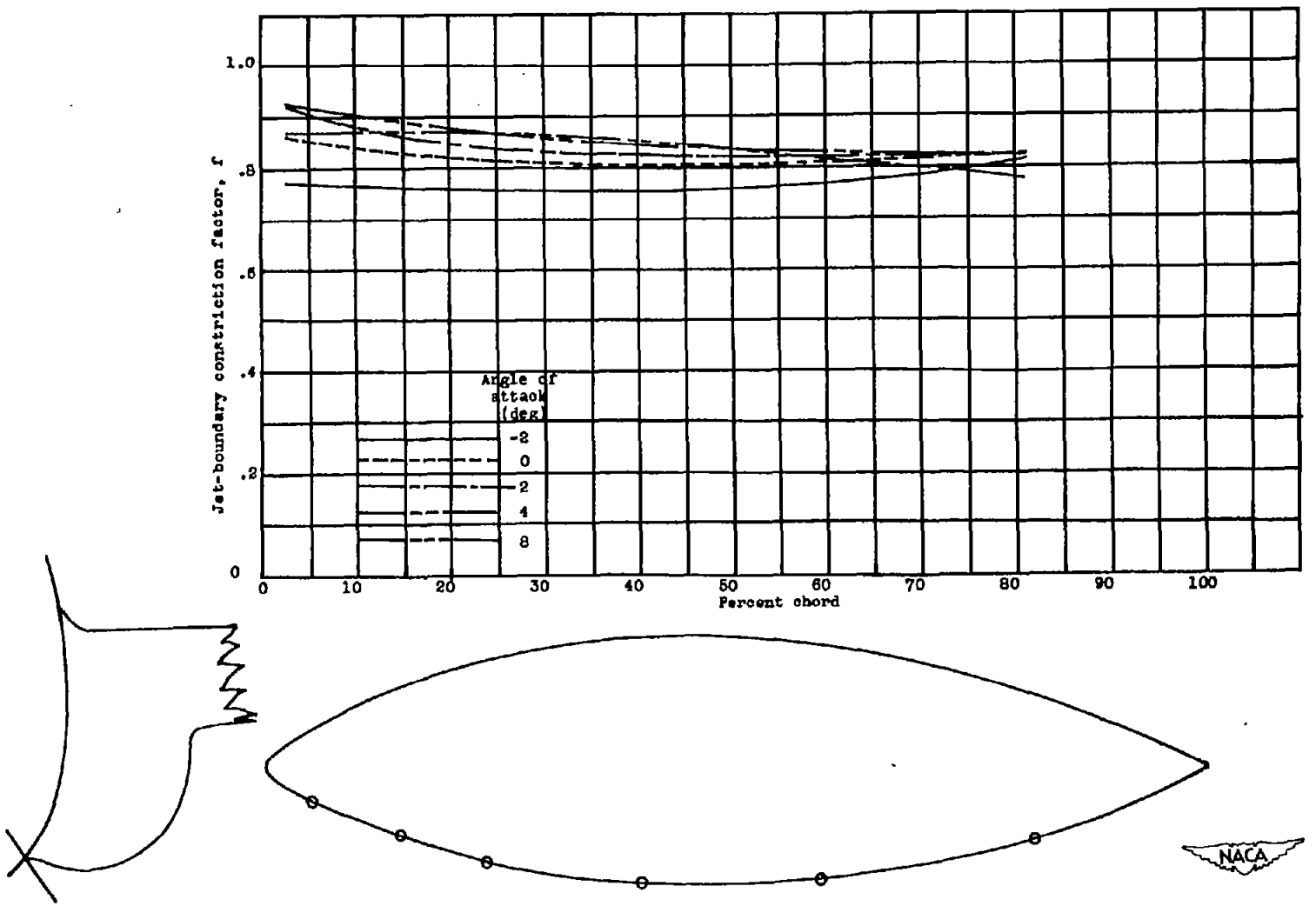

(j) Nacelles at section 4.

Figure 6. - Continued. Variation of jet-boundary constriction factor with angle of attack and chordwise location. (Orifice locations indicated on sketch.)

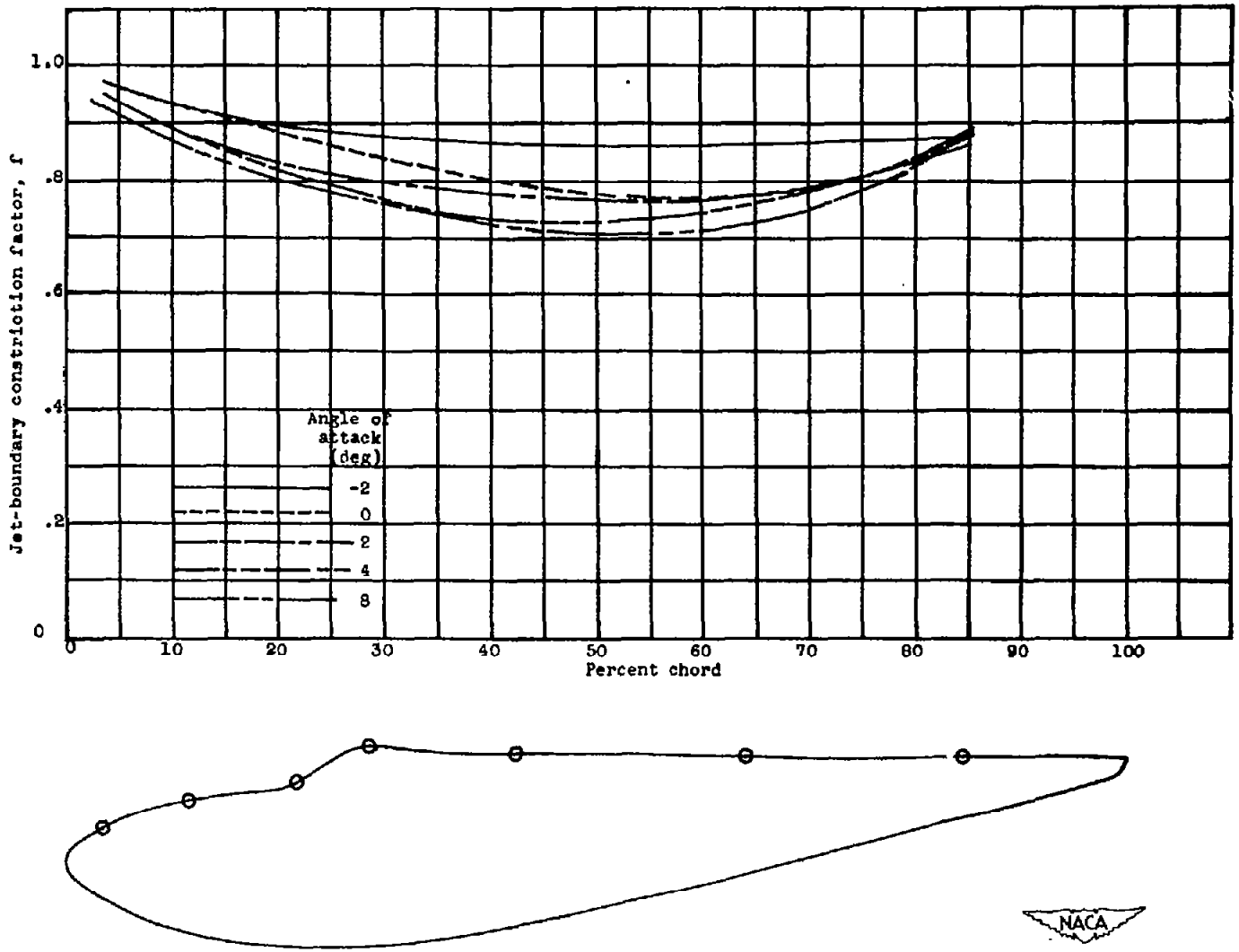

(k) Fuselage upper surface at section 6.

Figure 6. - Continued. Variation of jet-boundary constriction factor with angle of attack and chordwise location. (Orifice locations indicated on sketch.)

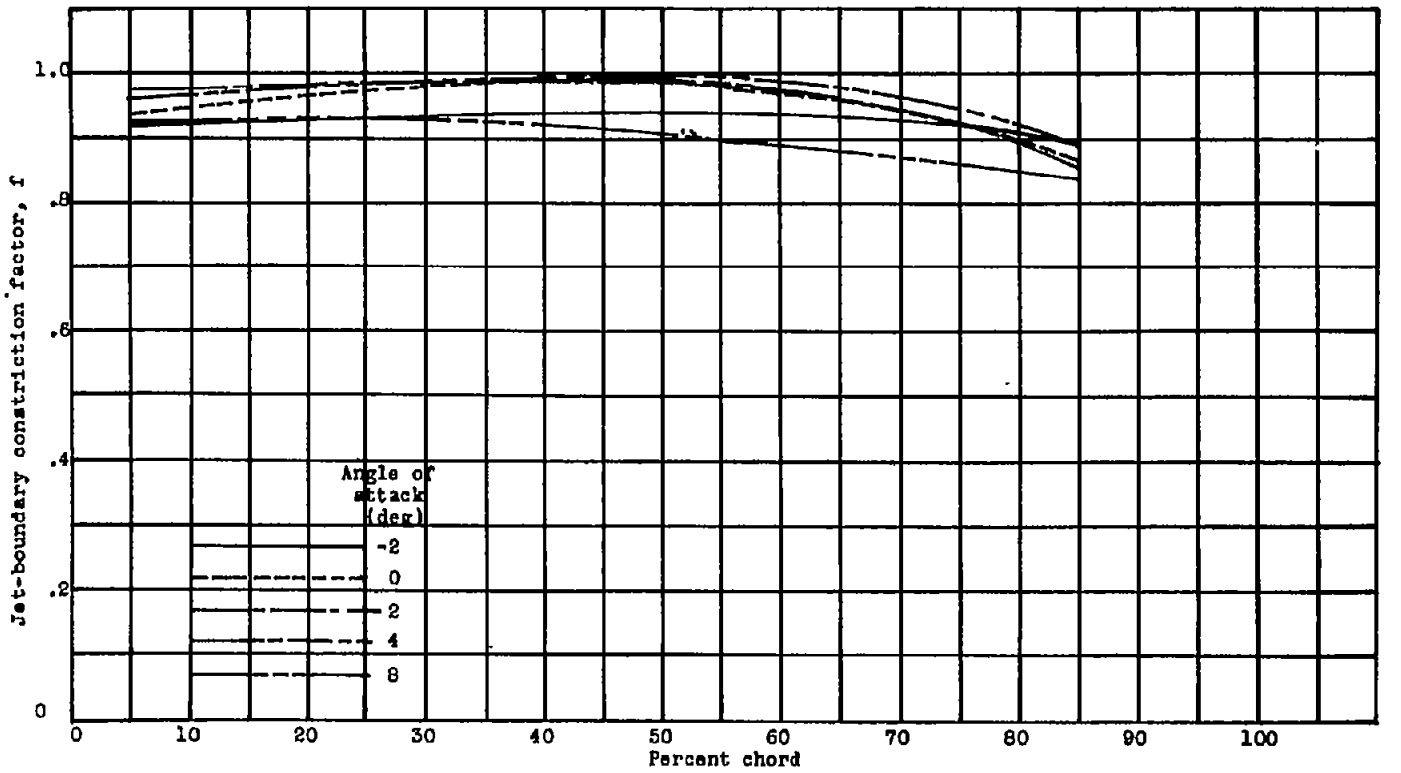

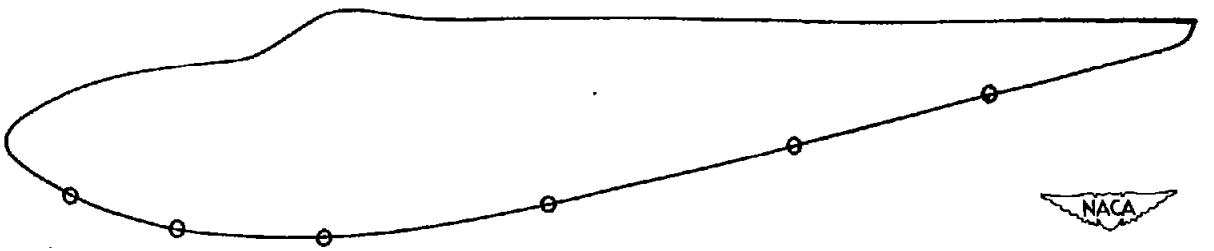

(l) Fuselage lower surface at section 5.

Figure 6. - Concluded. Variation of jet-boundary constriction factor with angle of attack and chordwise location. (Orifice locations indicated on sketch.)

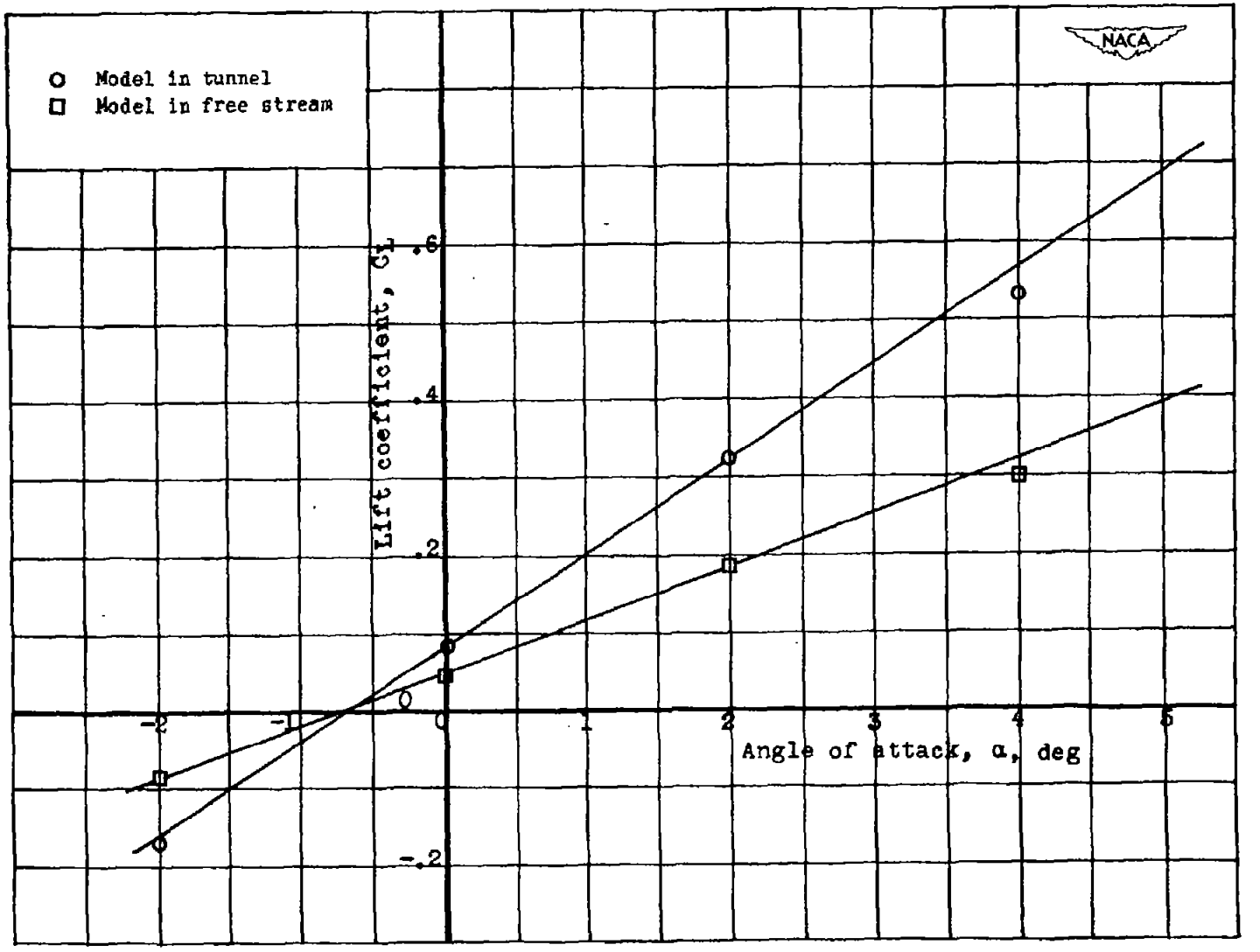

Figure 7. - Variation of model lift coefficient with angle of attack.